How dependent are quantitative volcanic ash concentration and along-flight dosage forecasts to model structural choices?

James, L. A. ORCID: https://orcid.org/0000-0002-7712-2837, Dacre, H. F. ORCID: https://orcid.org/0000-0003-4328-9126 and Harvey, N. J. ORCID: https://orcid.org/0000-0003-0973-5794 (2024) How dependent are quantitative volcanic ash concentration and along-flight dosage forecasts to model structural choices? Meteorological Applications, 31 (5). e70003. ISSN 1469-8080 doi: 10.1002/met.70003 Available at https://centaur.reading.ac.uk/118514/

Received: 10 April 2024 | Revised: 18 July 2024 | Accepted: 17 September 2024

DOI: 10.1002/met.70003

Meteorological Applications
Science and Technology for Weather and Climate
Open Access
RMetS

RESEARCH ARTICLE

How dependent are quantitative volcanic ash concentration and along-flight dosage forecasts to model structural choices?

Lauren A. James | **Helen F. Dacre** | **Natalie J. Harvey**

Department of Meteorology, University of Reading, Berkshire, UK

Correspondence
Natalie J. Harvey, Department of Meteorology, University of Reading, Berkshire RG6 7BE, UK.
Email: n.j.harvey@reading.ac.uk

Funding information
Lloyds Tercentenary Research Foundation

Abstract

Producing quantitative volcanic ash forecasts is challenging due to multiple sources of uncertainty. Careful consideration of this uncertainty is required to produce timely and robust hazard warnings. Structural uncertainty occurs when a model fails to produce accurate forecasts, despite good knowledge of the eruption source parameters, meteorological conditions and suitable parameterizations of transport and deposition processes. This uncertainty is frequently overlooked in forecasting practices. Using a Lagrangian particle dispersion model, simulations with varied output spatial resolution, temporal averaging period and particle release rate are performed to quantify the impact of these structural choices. This experiment reveals that, for the 2019 Raikoke eruption, structural choices give measurements of peak ash concentration spanning an order of magnitude, significantly impacting decision-relevant thresholds used in aviation flight planning. Conversely, along-flight dosage estimates exhibit less sensitivity to structural choices, suggesting it is a more robust metric to use in flight planning. Uncertainty can be reduced by eliminating structural choices that do not result in a favourable level of agreement with a high-resolution reference simulation. Reliable forecasts require output spatial resolution $\leq$ 80 km, temporal averaging periods $\leq$ 3 h and particle release rates $\geq$ 5000 particles/h. This suggests that simulations with relatively small numbers of particles could be used to produce a large ensemble of simulations without significant loss of accuracy. Comparison with previous Raikoke simulations indicates that the uncertainty associated with these constrained structural choices is smaller than those associated with satellite constrained eruption source parameter and internal model parameter uncertainties. Thus, given suitable structural choices, other epistemic sources of uncertainty are likely to dominate. This insight is useful for the design of ensemble methodologies which are required to enable a shift from deterministic to probabilistic

forecasting. The results are applicable to other long-range dispersion problems and to Eulerian dispersion models.

KEYWORDS

ash concentration, ash dosage, aviation, dispersion modelling, horizontal resolution, spatial resolution

1 | INTRODUCTION

The presence of volcanic ash poses a significant threat to aviation safety and operations, necessitating robust forecasting and warning systems. Many forecasts provide deterministic maps of ash concentrations, a critical factor in alerting flight operators to potential hazards (Beckett et al., 2020; Crawford et al., 2022; Gouhier et al., 2020; Zidikheri & Lucas, 2021). However, volcanic ash forecasting faces many challenges due to multiple sources of uncertainty (Harvey et al., 2018; Mastin et al., 2022). Thus, adhering to guidelines set by the International Civil Aviation Organization, the aviation industry is transitioning from deterministic to probabilistic forecasting. This probabilistic approach acknowledges the uncertainty in volcanic ash forecasts and will communicate the likelihood of exceeding predefined ash concentration thresholds (International Civil Aviation Organization, 2022).

To generate probabilistic quantitative volcanic ash forecasts, ensembles (multiple realizations of the forecast with plausible parameters) are typically employed to sample the uncertainty (Capponi & Saint, 2022; Dare et al., 2016; Harvey et al., 2020, 2022; Kristiansen et al., 2012; Webster & Thomson, 2022). There are three sources of epistemic uncertainty: input uncertainty, parametric uncertainty and structural uncertainty (Rougier & Beven, 2013). Input uncertainty stems from an incomplete understanding of the true value of the eruption source parameters (e.g., eruption magnitude and duration, plume height, composition and size of volcanic ash) and meteorological fields (e.g., 3D winds, precipitation). Parametric uncertainty occurs due to incomplete knowledge about the correct settings of the model's internal parameters (e.g., parameterized turbulence intensity, precipitation scavenging coefficients, dry deposition rates). Finally, structural uncertainty arises when the model fails to accurately represent the system, even with known correct parameters and inputs. For example, the choices of output resolution (spatial and temporal) and omission of physical processes such as ash particle aggregation, umbrella cloud spreading and other processes driven by the eruption dynamics (e.g., bent over plumes). Collectively, these sources form a comprehensive probabilistic description of a volcanic ash model's epistemic uncertainty. However, in practice, specifying these uncertainties proves exceedingly challenging and often involves a degree of subjectivity meaning that characterization of volcanic ash forecast uncertainties in an operational timescale remains a challenging task.

It is expected that flight planning and decision support systems for operators will increasingly make use of probabilistic quantitative volcanic ash forecasts to optimize airspace usage and plan more efficient routes during significant volcanic ash cloud events (International Civil Aviation Organization, 2022). The methodologies employed by operational centres to generate these forecasts will depend on factors such as computational resources, scientific understanding and technical proficiency. Previous studies have investigated the treatment of input and parametric uncertainty (Dacre & Harvey, 2018; Denlinger et al., 2012; Folch et al., 2012; Stefanescu et al., 2014), but structural uncertainty is frequently overlooked despite being highlighted as a source of uncertainty that should be considered (Folch, 2012). There are a few volcanic ash transport and dispersion model intercomparison studies (Heard et al., 2012; Kristiansen et al., 2012; Witham et al., 2007) which implicitly include structural uncertainty. However, due to their complexity, these studies cannot isolate different sources of uncertainty. One other study by Crawford (2020) does vary the horizontal resolution and number of particles released in simulations of the 2008 eruption of the Alaskan volcano, Kasatochi. However, the focus of their study is the development of a technique to reliably reconstruct particle density using a Gaussian mixture model rather than uncertainty quantification. In this study, we contribute to the scientific understanding of volcanic ash forecast uncertainty by designing an experiment aimed at quantifying the sensitivity of flight planning decisions to structural choices only, within volcanic ash dispersion forecasts. Additionally, we assess the magnitude of the estimated structural uncertainty and compare it to previous findings that quantified input and parametric uncertainty, thereby discerning their relative magnitudes.

Flight planning decisions are currently based on peak along-flight ash concentrations based on forecast ash

concentrations output every 6 h out to 24 h ahead (Webster et al., 2012). However, major engine manufacturers, such as Rolls-Royce, emphasize that damage can also result from prolonged exposure to low ash concentrations during flights (Clarkson & Simpson, 2017; Lekki et al., 2013). Recognizing that risks extend beyond peak concentrations, flight operators also need comprehensive information about the potential dangers associated with accumulated engine ash ingestion (dosage). In this study, focusing on the 2019 eruption of the Russian volcano Raikoke, we investigate the sensitivity of both along-flight peak ash concentration and dosage to structural uncertainty since both measures are necessary for effective decision-making. This eruption has been chosen as a focus for this study as ash emitted caused disruption to flights in the north Pacific region.

The paper is structured as follows; in Section 2 we introduce the Raikoke 2019 eruption, the dispersion model NAME and our experimental design, Section 3 describes the results of the experiment in which we quantify the uncertainty associated with model structural choices, finally in Section 4 we provide recommendations for the spatial and temporal resolution of output concentration data, and (for Lagrangian models) the associated minimum particle release rate required to allow operators to accurately calculate along-flight peak concentrations and dosage.

2 | METHODS AND DATA

2.1 | Raikoke 2019

This study focuses on the 2019 eruption of the Russian volcano Raikoke. Raikoke is an uninhabited island located at at 48.2° N, 153.3° E in the Sea of the Okhotsk in the northwest Pacific Ocean (See Figure 1). Its most recent eruption started on 21 June 2019 at approximately 18:00 UTC and continued for 12 h ending at approximately 06:00 UTC on 22 June 2019. It is estimated that ash was initially expelled to a height between 10 and 14 km (Global Volcanism Program, 2019a). Visible satellite suggests that there was an umbrella cloud that quickly advected eastwards. In the days following, the plume moved Easterly then turned North Easterly over the Pacific Ocean due the ash encountering an extratropical cyclone. There was moderate disruption of airspace due to the Raikoke eruption, with over 40 airplanes being diverted (Global Volcanism Program, 2019b). This eruption is being considered as it is one of the most recent

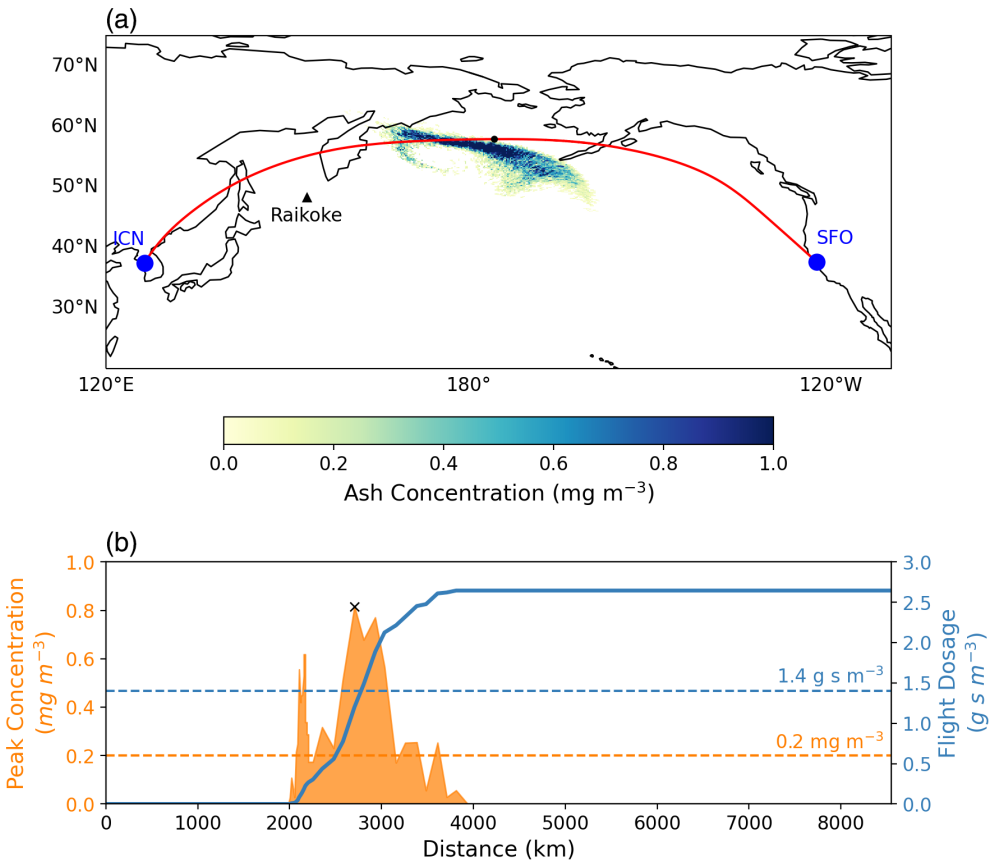

FIGURE 1 (a) NAME simulated ash concentration map between FL350–FL550 on 24 June 2019 00:00 UTC. A high-resolution model set-up is used; 20 km horizontal grid, 1 h averaging, 15,000 particles released per hour from the source during active release. The Raikoke volcano is depicted as a black triangle. The westbound flight route between San Francisco (SFO) and Seoul (ICN) is shown as a red line. The middle of the flight route is marked with the black dot. (b) Along-flight ash concentration (orange) and dosage (blue) encountered on the westbound flight route as a function of flight distance. Peak ash concentration encountered along the flight is represented by the black cross. Relevant ash concentration and dosage thresholds are shown as dashed horizontal lines.

eruptions that deposited ash into the stratosphere and the relatively simple meteorological situation following the eruption.

2.2 | NAME

In this study version 7.2 of the Numerical Atmospheric-dispersion Modelling Environment (NAME; Jones et al., 2007) is used. NAME is a Lagrangian particle dispersion model that is also used to produce the simulations used by the London Volcanic Ash Advisory Centre (LVAAC), which form the basis of volcanic ash forecasts for the aviation industry. The transport of ash is primarily driven by 3D winds from a numerical weather prediction model coupled with parameterizations of free tropospheric turbulence and mesoscale motions. The removal of ash from the atmosphere is modelled using parameterizations of sedimentation and dry and wet deposition. In this study, it is assumed that the ash particles have a density of 2300 kg m^{-3} and are spherical. The particle size distribution used is based on data from Hobbs et al. (1991). NAME does not currently include a parameterization for aggregation of ash particles or explicitly model near source plume rise or eruption dynamics.

2.3 | Simulation set-up for the Raikoke 2019 eruption

To simulate the Raikoke eruption, a constant plume height of 12.45 km was used and the Mastin relationship (Mastin et al., 2009) was used to determine the mass eruption rate. This was applied between 1800 UTC 21 June 2019–0600 UTC 22 June 2019. This is consistent with other studies of this eruption and observations of the eruption column (Bruckert et al., 2021; Capponi et al., 2022; Harvey et al., 2022; Muser et al., 2020; Prata et al., 2022). The meteorological data used to drive these simulations is from the deterministic Met Office Global analysis and forecast (Walters et al., 2019) and has a horizontal resolution of approximately 10 km and 70 vertical levels. The NAME simulations performed in this study update the meteorological data every 3 h.

Ash concentrations are calculated by summing the mass over a user defined volume by specifying a vertical and horizontal grid spacing. Time averages are produced using 10-min averaged data (i.e., a temporal averaging period of 1 h will use six model concentration values to estimate the ash concentration in a grid box). To account for loss processes near the volcano vent a distal fine ash fraction (DFAF) of 5% is applied (Beckett et al., 2020).

2.3.1 | Structural choices

Currently the operational set-up used by the LVAAC has a horizontal output grid spacing of 0.3 latitude × 0.5 longitude (approximately equivalent to 40 km grid boxes in the mid-latitudes), 6 hourly temporal averaging period and a particle release rate of 15,000/h (Beckett et al., 2020; Witham et al., 2019). However, the impact of these choices of output resolution and particle release rate on the resulting ash concentration has not been published in the scientific literature. To assess the sensitivity to these structural choices, simulations with varying output horizontal grid resolution, temporal averaging period and particle release rate have been performed. The following values have used in this study:

- Temporal averaging of 1, 2, 3, 6, 12 and 24 h
- Horizontal grid of 20, 40, 80 and 160 km
- Particle release rate of 1000, 5000, 10,000, 15,000 and 20,000 per h

Each parameter is varied independently, resulting in 120 simulations in total. The resulting simulations are compared to a high resolution control simulation which uses a horizontal grid of 20 km, temporal averaging period of 1 h and a hourly particle release rate of 15,000.

2.4 | Determination of peak ash concentration and dosage

To relate to flight routes and products currently produced by LVAAC, we restrict the analysis presented in this study to ash found between FL350 and FL550. This corresponds to cruise altitude for both transatlantic and transpacific flights. In our simulations ash concentrations are calculated on a vertical grid with 22 flight levels (FL) from FL000 to FL550 with a vertical resolution of 25FL. As in Prata et al. (2019) and Webster et al. (2012) these 'thin' layers are aggregated onto the three FL ranges used by the LVAAC (FL000–FL200, FL200–FL350 and FL350–FL550). The maximum ash concentration of the 'thin' layers (25FL thickness) within each range is used as the concentration of the associated 'thick' layer. The averaging performed within NAME to calculate ash concentrations results in NAME under-predicting the actual peak concentrations in the atmosphere. Thus, a scaling factor representing the ratio of the peak concentration to the resolved mean concentration is applied to the ash concentration output. This is known as a peak-to-mean factor (Webster et al., 2012). As in Prata et al. (2019), a peak-to-mean factor of 10 is applied (Webster et al., 2012). Note, however, that since we are interested

in the spread of ash concentration and dosage values rather than their absolute value in our study, this scaling does not affect the results.

From 2025 onwards, quantitative volcanic ash forecasts describing the exceedance frequency of peak ash concentration threshold values will be required (International Civil Aviation Organization, 2022). These threshold values are 0.2, 2.0, 4.0 and 10.0 mg m^{-3}. In this study we use these values to assess the implication of structural uncertainty for decision-making.

Flight dosage is the total amount of ash encountered along the flight path, measured in units of g s m^{-3}. This considers the ash concentration and the duration of the flight. The dosage, D, is calculated using the equation:

$$D = \sum_{i=1}^{n} C_i \Delta t_i = \sum_{i=1}^{n} C_i \frac{\Delta s_i}{V_a} \quad (1)$$

where n is the number of model grid boxes along the flight route, C_i is the ash concentration in the ith grid box, Δt_i is the duration of exposure to the ith grid box, Δs_i is the distance travelled through the ith grid box and V_a is the true air speed of the flight (Prata et al., 2019). The true air speed is the flight speed relative to the air being flown through. This can be considered the speed on ground with no wind.

An aeroplane can encounter a varying amount of ash depending on the dispersion of the plume and the relative location of the flight. In addition to the peak ash concentration encountered along a flight, flight operators require information about the risk of flying through low ash concentrations for long durations. Dosage is a measurement to aid this. Threshold levels have also been identified for dosage values that advise consideration of risk mitigation techniques. The threshold levels used here are 1.4, 14.4 and 28.8 g s m^{-3} (Capponi et al., 2022; Prata et al., 2019). These are equivalent to flying through a concentration of 2 mg m^{-3} for 0.2, 2 and 4 h respectively. Thus different dosage thresholds are expressed as diagonal lines on Duration of Exposure v Ash Concentration (DEvAC) charts (Clarkson et al., 2016).

2.5 | The relationship between peak ash concentration and dosage

Dosage is the accumulated product of ash concentration, C_i, and duration of exposure, Δt_i, (Equation 1). Thus it is possible to obtain high dosage values for flights encountering relatively low ash concentrations for an extended period of time. In this section we examine the relationship between peak concentration and dosage. A high correlation implies that these two variables can be used interchangeably, a low correlation suggests that both peak concentration and dosage should be considered in parallel when making flight planning decisions.

To evaluate the along-flight peak ash concentration and dosage, a flight path between San Francisco (SFO), United States, and Seoul (ICN), South Korea is considered. This route travels over the North of the Pacific Ocean, encountering volcanic ash (Figure 1a). To calculate dosage, we assume a flight true air speed, V_a, of 240 m s^{-1}.

Figure 1b shows the ash concentration along the flight trajectory and the accumulated flight dosage for a flight on 24 June at 00:00 UTC, 54 h after the eruption started. A threshold of 0.2 mg m^{-3} is exceeded for a section of the flight, between 2000 and 3500 km (equivalent to 17% of the flight distance). A peak concentration of 0.8 mg m^{-3} is encountered 2700 km along the flight route (Figure 1, black cross). The dosage threshold of 1.4 g s m^{-3} is exceeded on this route from approximately 2700 km onwards (equivalent to 68% of the flight route).

Next we consider the relationship between peak concentration for multiple flight routes through the ash cloud at cruise level. Rather than calculate multiple flight routes we simply rotate the existing ash cloud about a local origin. This is equivalent to approaching and flying through the ash cloud from different angles. The rotation point is mid-flight path at 57.9° latitude and 184.3° longitude (Figure 1a, black dot).

Figure 2a presents the relationship between peak ash concentration and dosage obtained along each flight route. The calculated correlation coefficient (r^2 value) of 0.17 suggests a weak positive correlation. Displaying the data as a probability distribution function enables the distribution of these measurements to be seen clearly (Figure 2b,c). Zero values of both peak concentration and dosage are removed. A kernel density fit to the data shows a significant difference in the distribution of peak ash concentration and dosage. The peak concentration displays a uni-modal distribution (Figure 2b) but the dosage has a bimodal distribution (Figure 2c). At this model time, the ash region is elongated along the south-east to north-west axis, and contracted along the the south-west to north-east axis (Figure 1a). Flights that are more aligned with the south-east to north-west axis (in either direction) will encounter the ash cloud for a long duration resulting in high dosage values. Flights that are more aligned with the south-west to north-east axis will encounter the ash cloud for a short direction resulting in relatively low dosage values. This results in a bimodal distribution of dosage. However, different flight orientations may fly through or either side of the region of highest ash concentrations, resulting in a uni-modal peak ash concentration distribution.

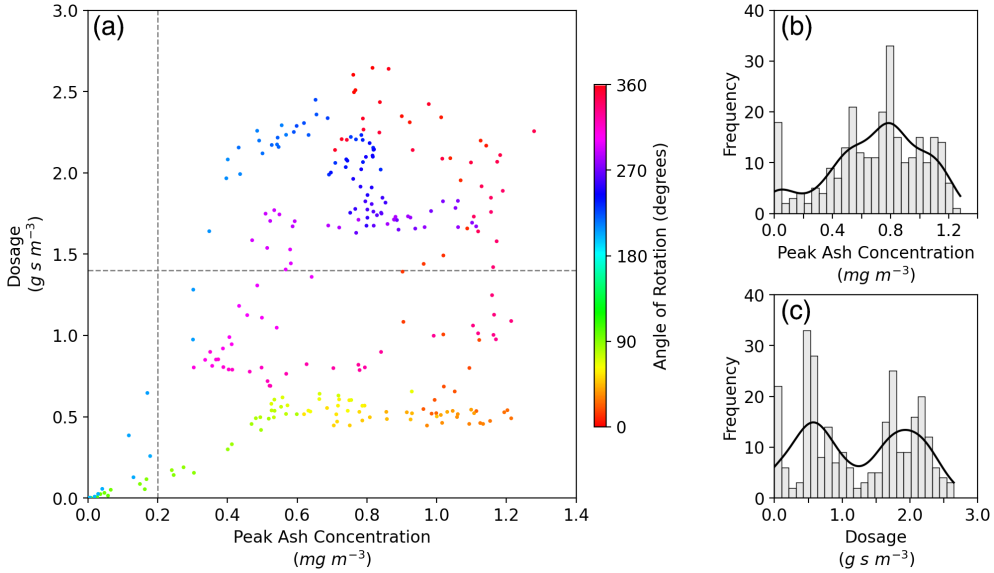

FIGURE 2 Distribution of the peak ash concentration and dosage for 360 flights through the ash at FL350–FL550 on 24 June 2019 00:00 UTC. (a) The distribution of data in relation to peak concentration threshold of 0.2 mg m^{-3} and dosage threshold of 1.4 g s m^{-3}. The colour of the dot corresponds to the angle of the flight route, measured anticlockwise from true North. (b) Probability distribution function of peak ash concentration >0.0 mg m^{-3}, fitted with a kernel density estimate (solid line). (c) Probability distribution function of dosage >0.0 g s m^{-3}, fitted with a kernel density estimate (solid line).

This highlights that peak ash concentration is not a good proxy for along-flight dosage. Of the 360 flight routes considered, 245 flights (68.0%) exceed the lowest peak ash concentration threshold of 0.2 mg m^{-3}. A total of 128 flights (35.6%) exceed the lowest dosage threshold of 1.4 g s m^{-3}, a reduction of 52.2% of flights that would potentially be considered as hazardous to aviation.

3 | RESULTS

In this section we quantify the sensitivity of peak ash concentration and dosage to different choices of model structural set-up. Three model structural choices (output horizontal grid resolution, output temporal averaging period and particle release rate) are varied one-at-a-time (OAT) to quantify the possible maximum and minimum range of along-flight peak concentration and dosage estimated by NAME. In addition, all three parameters are varied at the same time (multivariate sensitivity) and compared to the OAT sensitivity analysis to evaluate dependence between structural choices.

3.1 | Evolution of peak ash concentration and dosage

Figure 3 shows the range of values for westbound flights between San Francisco (SFO) and Seoul (ICN) departing every 6 h after the start of the eruption. For output temporal averaging periods longer than 6 h, peak ash concentration and dosage values are assumed to remain constant for the respective temporal averaging periods.

Figure 3a,b show peak ash concentration and dosage for the SFO-ICN flights. Peak ash concentration and dosage show a similar temporal variability, with high peak ash concentration periods typically coinciding with high ash dosage periods and vice versa. However, there is a noticeable distinction in the structural choice to which these two measurements show the highest sensitivity. The number of particles released is particularly influential for estimations of peak concentration due to stochastic uncertainty in the concentration values when there are very few particles in a geotemporal grid box. The dosage is less sensitive to the number of particles since it is a path integrated quantity. Dosage is most influenced by output temporal averaging period. Larger output temporal averaging periods typically result in the total ash mass in the atmosphere being spread over larger volume. In a given grid box this can result in an increase or decrease in concentration, C_i, which may impact dosage if the flight path coincides with the gridbox (Equation 1).

As a result of these structural choices, obtained measurements of peak ash concentration can range over an order of magnitude, spanning decision relevant threshold values at specific times. For example, on 24 June 06:00 UTC it is possible to obtain peak ash concentration levels ranging from 0.2 to 2.0 mg m^{-3} thresholds. Conversely,

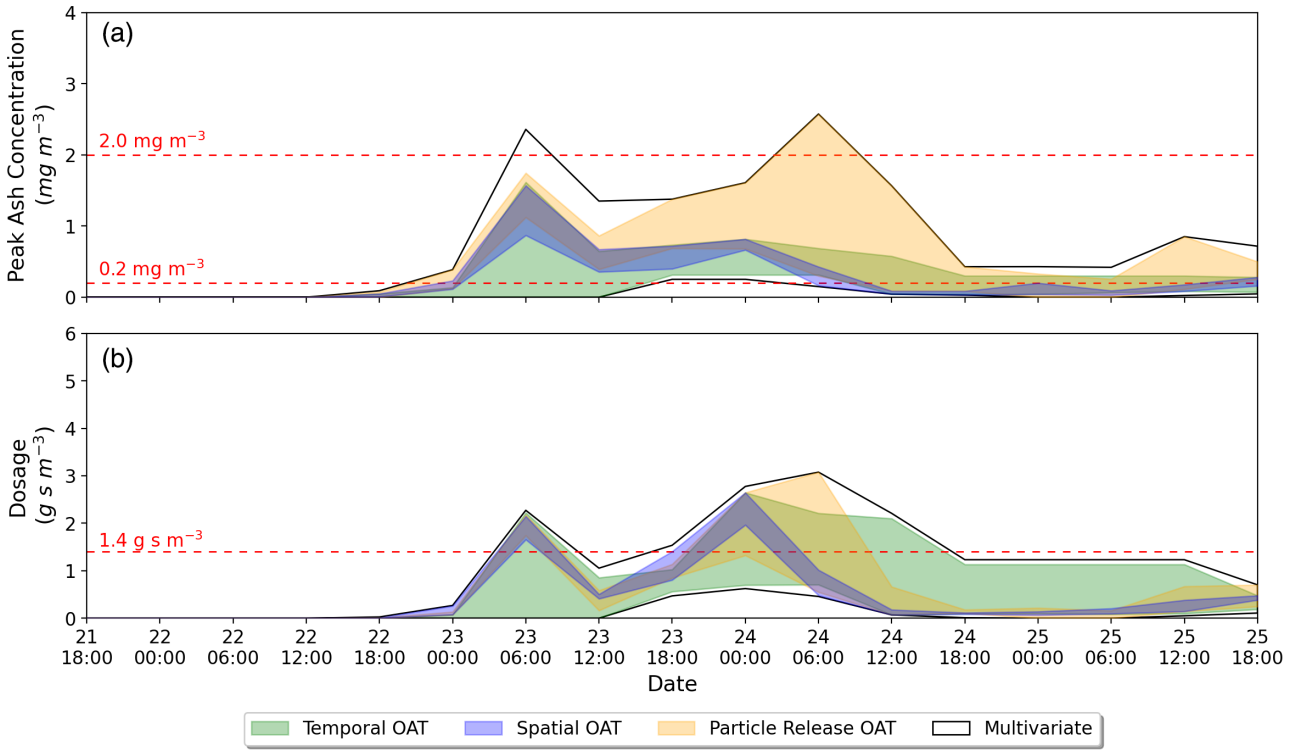

FIGURE 3 Along-flight peak ash concentration (a) and dosage (b), for westbound flights between San Francisco and Seoul departing every 6 h after the start of the eruption. Spread of values resulting from One-At-a Time (OAT) simulations varying horizontal grid resolution (blue shading), temporal averaging period (green shading) and hourly particle release rate (yellow shading). Maximum and minimum values from multivariate sensitivity analysis to all three parameters (black solid lines). Relevant threshold limits are indicated by horizontal red dashed lines.

dosage estimates typically range over a factor of 2 or 3 only.

For both peak ash concentration and dosage, the multivariate analysis demonstrates that, for certain flights, model set-up choices can interact to increase the uncertainty range. For example, at 06 UTC on 23 June 2019 a combination of model set-up choices results in estimated peak concentration values that exceed the 2 mg m^{-3} threshold used in aviation flight planning whereas the OAT testing do not.

3.2 | Finding acceptable structural choices

In this section we compare the peak concentration and dosage values for each of the 120 NAME model simulations against the simulation with the highest output spatial and temporal resolution and a high particle release rate (20 km spatial resolution, 1 h temporal averaging, 15,000/h particle release rate), hereafter the control simulation. Here, the values from the simulations with the range of structural choices outlined in Section 2.3.1 are said to agree with the control simulation if they are within a factor of 2 of the control simulation. Here, we define FAC2 as the percentage of values that satisfy the criteria,

$$0.5 \leq C_i / C_c \leq 2.0, \tag{2}$$

where C_i is the time series of 6-hourly peak concentration and dosage values from a simulation with a specific set of structural choices and C_c is the equivalent from the control simulation. By definition, the control simulation has a FAC2 value of 100% (hatched squares in Figure 4).

In Figure 4, the ability of each simulation to estimate the peak ash concentration and dosage is displayed as heat maps. Pale shades correspond to a high FAC2, and dark shades correspond to a low FAC2. Each heat map (6 × 4 grid) represents a constant hourly particle release rate with variation of the output temporal averaging period and the output horizontal grid resolution presented on the axis.

There is clear similarity in pattern between the heat maps in which particle release rate exceeds 1000 particles per hour (Figure 4 1B–E and 2B–E), suggesting relatively small impact from varying the particle release rate above this threshold. Whilst some simulations initiated with a

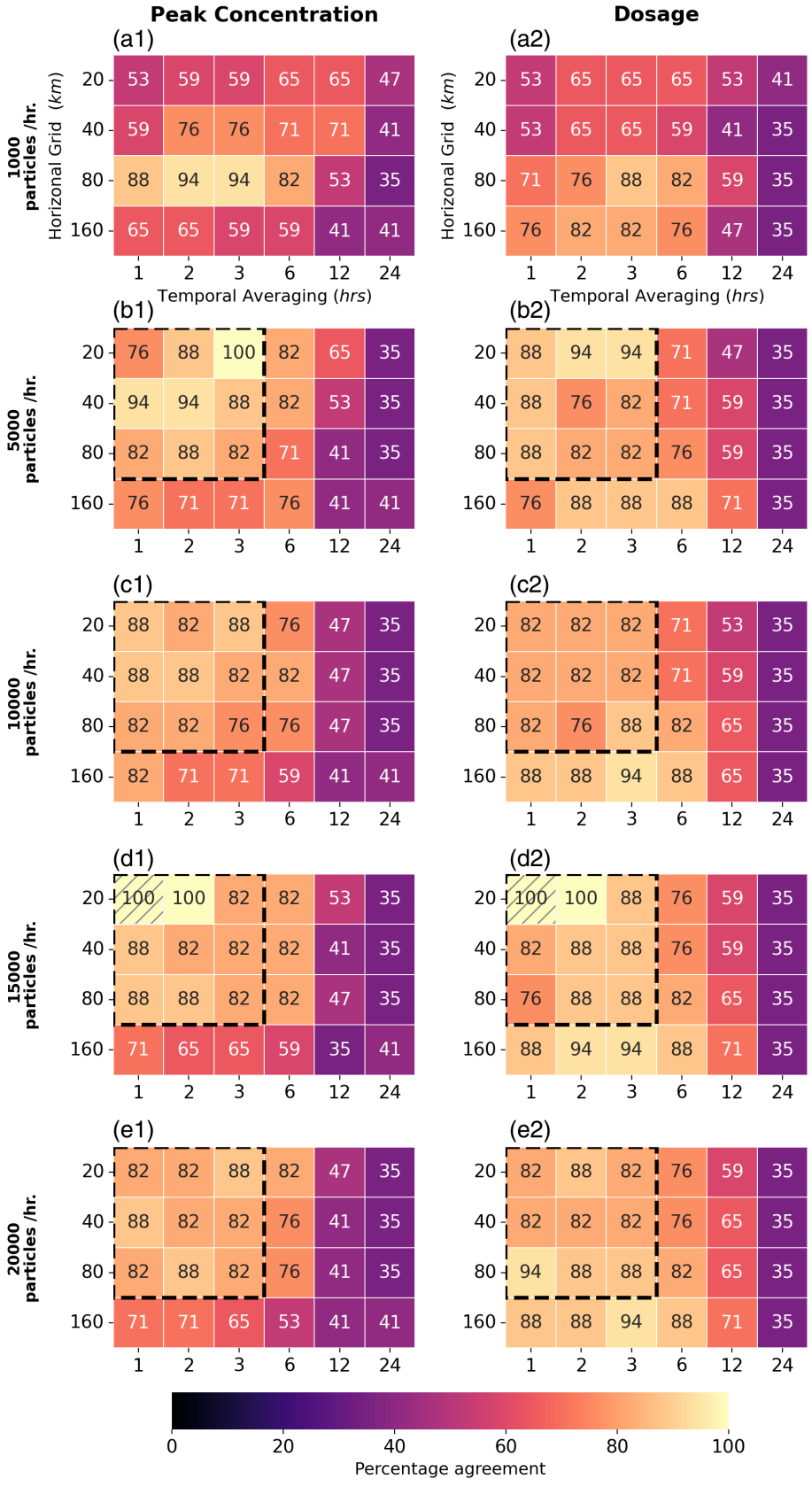

FIGURE 4 FAC2 (Equation 2) for along-flight peak ash concentration (left column) and dosage (right column) for all 120 model structural choices. Each heat map displays FAC2 for varying temporal averaging period and the horizontal grid resolution, but fixed hourly particle release rate. The different particle release rate simulations are shown from top to bottom (a–e). The same colour scale is used in all heat maps; pale shades correspond to a high FAC2 while dark shades correspond to low FAC2. Model structure setup choices that are identified as being suitable alternatives to the control simulation (hatched box) are contained within the boxes indicated with dashed black lines.

release rate of 1000 particles per hour obtain good agreement with the control run (FAC2 $\geq$ 75%, Figure 4 1A,2A), the sensitivity to different structural choices appears noisy. Thus, we consider model set-up with 1000 particles/h contain too few particles to produce a reliable estimate of peak concentration. Note that the simulations

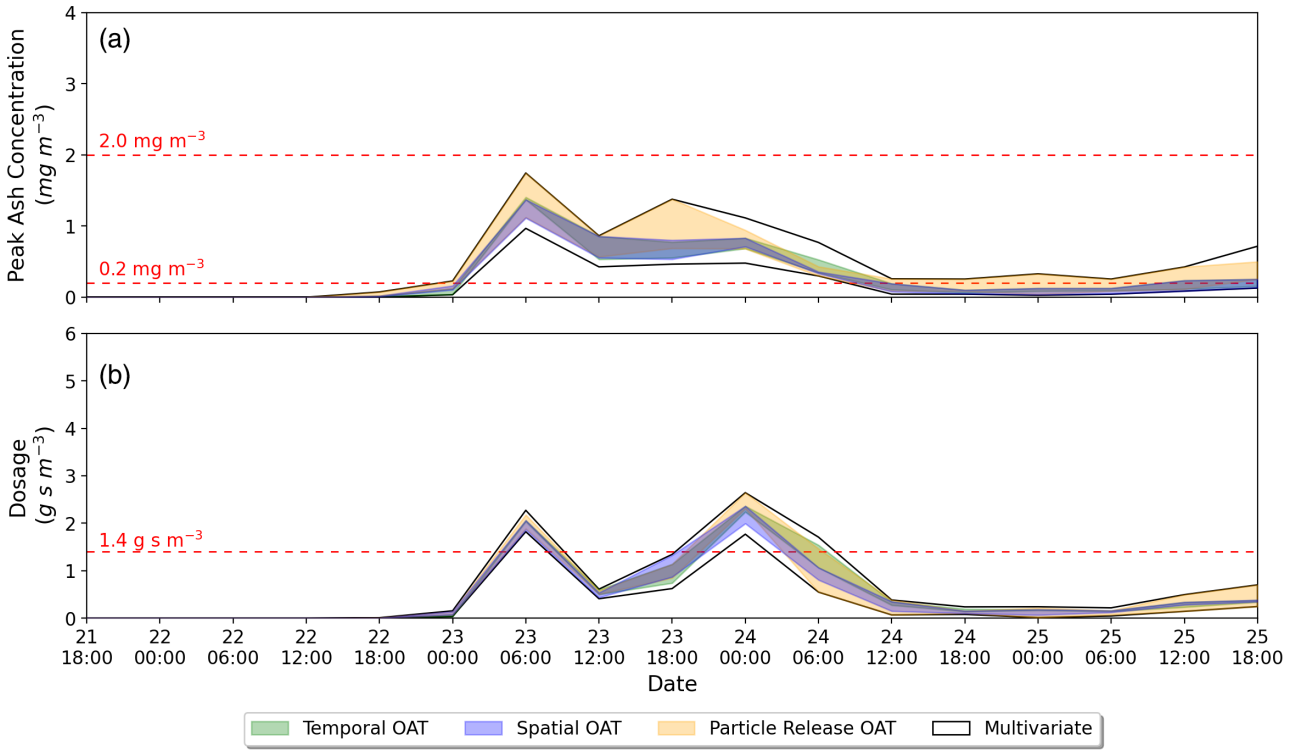

FIGURE 5 Along-flight peak ash concentration (a) and dosage (b), for westbound flights between San Francisco and Seoul departing every 6 h after the start of the eruption. One-At-a Time (OAT) sensitivity to varying parameters within the reduced parameter space are shown for horizontal grid resolution (blue shading), temporal averaging period (green shading) and hourly particle release rate (yellow shading). Maximum and minimum values from multivariate sensitivity analysis of all three parameters within the reduced parameter space are also shown (black solid line). Threshold limits are indicated by horizontal red dashed lines.

with 5000 particles/h are typically three times faster to run than those with 15,000 particles/h so it is notable that FAC2 $\geq 75\%$ can still be achieved with the computationally cheaper simulations (with appropriate output spatial resolution and temporal averaging).

The choice of output temporal averaging period (*x*-axis in Figure 4) has significant impact on the performance of the simulation for both peak concentration and dosage estimates. An output time averaging period of 6 h or longer leads to a FAC2 ranging from 35%–82% for along-flight peak ash concentration estimates. Similarly, FAC2 for the flight dosage estimates with averaging periods of 6 h or longer range from 35%–88%, with 12 and 24 h temporal averaging producing FAC2 $\leq$ 71%. FAC2 for averaging periods $\leq$3 h do not vary significantly. This suggests that output temporal averaging periods of 3 h or shorter are required to give reliable estimates of peak concentration and dosage.

Finally, the choice of output horizontal grid resolution (*y*-axis in Figure 4) shows the smallest variability for peak concentrations and almost no variability for dosage. Decreasing the horizontal resolution decreases FAC2, but by only a few percent (for particle release rates greater than 1000 particles/h). FAC2 falls below 75% for peak concentration estimates using the coarsest output horizontal resolution (160 km) suggesting that this is not an appropriate structural choice. Conversely, FAC2 remains relatively high for dosage values.

Based on this analysis, the structural uncertainty in peak concentration and dosage forecasts can be reduced by eliminating model choices that do not result in an accurate representation of peak concentration or dosage. The restricted parameter values are hourly particle release rate of 5000, 10,000, 15,000 and 20,000; temporal averaging period of 1, 2 and 3 h and a spatial resolution of 20, 40 and 80 km. These 36 model set-up choices are highlighted in Figure 4 by dashed black boxes. Within the reduced parameter space, the FAC2 of along-flight peak ash concentration and dosage is $\geq$ 76%.

The uncertainty of the reduced-parameter sensitivity simulations as a function of time is shown in Figure 5. As expected, the uncertainties in estimates of peak ash concentration and dosage are reduced throughout the time series. In general, all model runs agree on the threshold exceedance for along-flight peak ash concentration and dosage. Thus, these choices of structural set-up result in the reduced impact of structural uncertainty in the decision-making process.

It is noted that the new ICAO guidance stipulates that forecast data is available at a horizontal resolution of 0.25 latitude × 0.25 longitude horizontal grid. This resolution is situated between the 20 and 40 km spatial scale presented here. The guidance does not refer to a temporal averaging period. However, the guidelines stipulate that forecasts are available at 3-h increments and it would be unlikely for the averaging period to exceed this time period.

3.3 | Comparison with other sources of uncertainty

In addition to structural uncertainties associated with the model set-up choices, there are several other sources of uncertainty. For example, uncertainties in the input 3D wind fields and precipitation, the eruption source parameters and internal model parameterizations such as the representation of turbulence and deposition. In this section we compare the structural uncertainty to other epistemic sources of uncertainty.

Capponi et al. (2022) performed NAME ensemble simulations by perturbing nine parameters associated with meteorological, eruption source parameter and internal model parameter uncertainty. For the 2019 Raikoke eruption 11 1000-member ensembles were performed iteratively. Each iteration uses satellite observations to constrain the range of potential values for each input parameter. Satellite observations from 24 June 2019 00:00 UTC were used to constrain the eighth iteration of ensembles, hereafter ENS08 (Capponi & Saint, 2022). Table 1 shows the parameters varied and their ranges for ENS08. These parameters were chosen to be varied following Harvey et al. (2018) and Prata et al. (2019). It is interesting to note that there are a wide range of parameters that give outputs that are considered a close enough match to the satellite observations of ash column loading. For all 1000 members in ENS08, the peak ash concentration and dosage along the SFO-ICN route are calculated every 6 h. In Figure 6, the constrained time series of structural uncertainty is compared to the ensemble range obtained from ENS08.

First we compare the temporal evolution of peak ash concentration and dosage for the SFO-ICN flights (Figure 6). Both the peak concentration and dosage show a delayed encounter with the ash cloud in the ENS08 simulations (occurring for flights departing 18 h later) compared to the results in this study. As stated above, the ENS08 simulations are constrained by satellite observations. Capponi et al. (2022) (their Figure 8C) show that the satellite does not detect ash cloud in the vicinity of the flight path at earlier times resulting in parameter values causing dispersion to this location being eliminated by the satellite information.

TABLE 1 Parameters sampled and their control and sampling ranges for ENS08 in Capponi and Saint (2022).

Parameter	Control value	Sampling range in ENS08
Plume height (km)	12.45	9.12–26.91
MER factor	1	0.3–2.2
Ash density (kg m^{-3})	2300	1120–2630
Source duration (h)	12	8–24
Distal fine ash fraction (%)	5	0.55–37.38
Horizontal (vertical) Lagrangian timescale for free tropospheric turbulence (s)	300 (100)	100–899 (33–299)
Standard deviation of horizontal (vertical) velocity for free tropospheric turbulence (m s^{-1})	0.25 (0.1)	0.0025–2.7 (0.0001–0.11)
Standard deviation (σ) of horizontal velocity for unresolved mesoscale motions (m s^{-1})	0.8	0.27–1.74
Meteorological fields	Met office unified model global analysis	Met office global and regional ensemble prediction system members 0–17

Next we compare the uncertainty in peak concentration and dosage between the ENS08 simulations and the results in this study. The uncertainty associated with structural choices in the model (Figure 6, black lines) is smaller than those associated with the constrained eruption source parameter values and internal model parameters (Figure 6, grey hatching). This suggests that, given suitable choices for particle release rate, output temporal and spatial resolution, other epistemic sources of uncertainty (e.g., meteorological situation, plume height, ash composition and representation of loss processes) are likely to dominate peak concentration and dosage predictions.

4 | CONCLUSIONS

This study presents an evaluation of the uncertainty in volcanic ash concentration and along-flight dosage caused by the structural choices within NAME. A suite of simulations of the 2019 eruption of Raikoke are

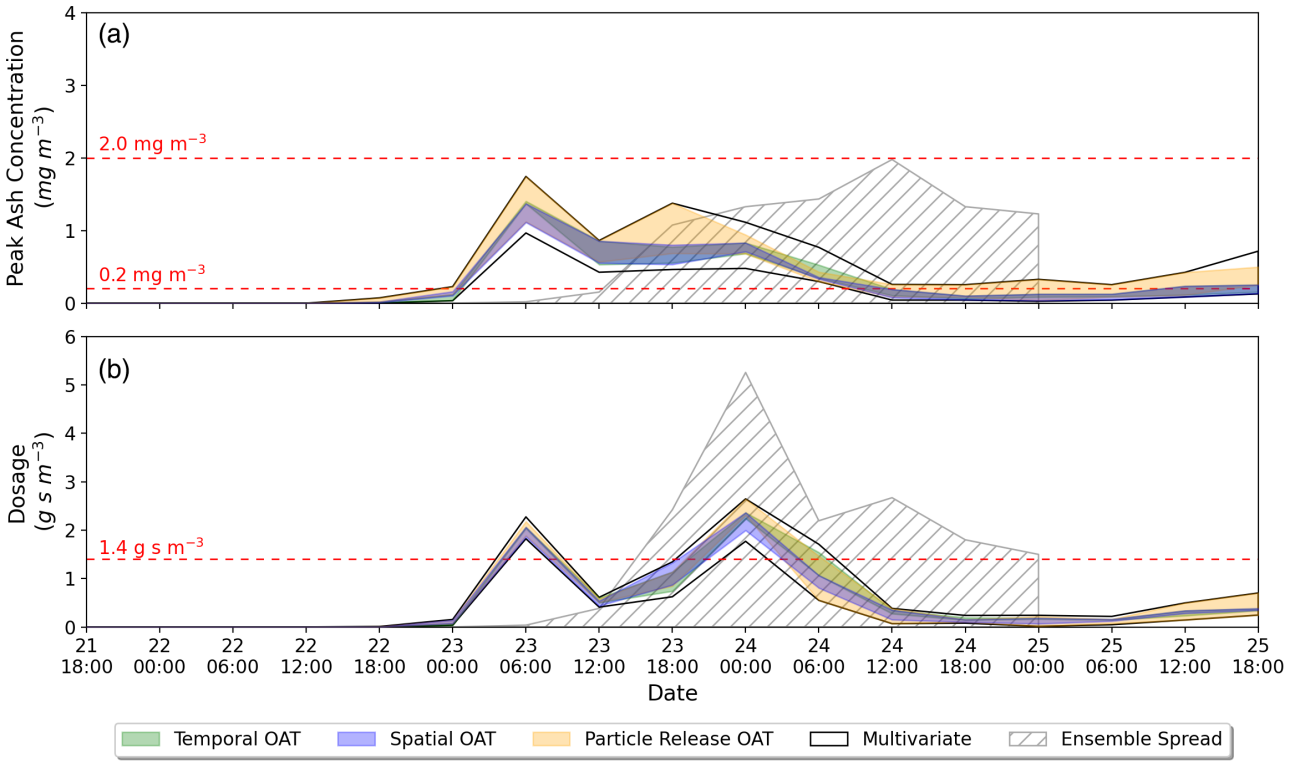

FIGURE 6 As Figure 5 but with ensemble data (ENS08) from Capponi et al. (2022) overlaid (hatching). ENS08 has been confined using satellite observations from 24 June 00:00 UTC and dispersion is only tracked between 22 June 12:00–25 June 00:00. Threshold limits are indicated by horizontal red dashed lines.

performed, and peak ash concentrations and along-flight dosages along a westbound flight from San Francisco to Seoul are calculated for FL350-500 (cruise altitude). A high-resolution simulation with a horizontal resolution of 20 km, temporal averaging of 1 h and a particle release rate of 15,000 per hour is used as a control. In the control simulation, at 00:00 UTC on 23 June 2019 the flight encounters ash with peak concentration of 0.8 mg m^{-3} and a dosage of 2.6 g s m^{-3}. These values are both above the thresholds used to indicate the presence of ash by ICAO (International Civil Aviation Organization, 2022).

To assess the relationship between peak ash concentration and along-flight dosage we calculate these quantities for multiple flight routes through the same ash cloud. A range of values were found for both quantities with 245 (68.0%) flights exceeding the 0.2 mg m^{-3} ash concentration threshold and 128 (35.6%) flights exceeding the 1.4 g s m^{-3} dosage threshold. There is a weak correlation between peak ash concentration and dosage demonstrating that both quantities should be considered when making operational flight planning decisions. This supports the work in Clarkson et al. (2016) that advocates the use of dosage as a suitable metric for flight planning.

Analysis of a set of simulations that vary the number of Lagrangian particles released per hour (1000–20,000/h), output horizontal grid resolution (20–160 km) and temporal averaging period (1–24 h) has been performed. The range of structural choices that are suitable for forecasts of volcanic ash for aviation purposes is determined by comparison to the high-resolution reference simulation. Peak ash concentration is influenced most by the number of particles released per hour whereas dosage is influenced most by the temporal averaging period used.

Analysis of 17 flights, departing every 6 h after the start of the eruption, shows that structural parameters within the range 1–3 h temporal averaging, 20–80 km horizontal grid and $\geq$ 5000 particles released per hour produce a good estimate of both the along-flight measurements. Simulations with these choices result in $>75\%$ of peak concentration and along-flight dosage estimates that are within a factor of 2 (FAC2) of the reference simulation. Along-flight dosage is less sensitive to the structural choices considered here than peak concentration. This suggests that dosage is potentially a more robust metric to use for flight planning as it is not influenced as much as concentration by structural choices. It is also interesting to note that FAC2 $>75\%$ can be achieved with a particle release rate of 5000/h. These simulations are typically three times faster to run than those with 15,000 particles per hour. This suggests that

one strategy for producing large ensembles needed to create probabilistic forecasts may be to perform multiple cheaper simulations with smaller numbers of particles than are currently used in the deterministic set-up.

When comparing the impact of structural choices on the peak concentration and dosage to the range found using an ensemble of simulations that perturb nine eruption source and internal model parameters produced for Capponi et al. (2022), it is found that structural uncertainty is smaller but not insignificant (up to approximately 20%) for both quantities. Thus, other sources of epistemic uncertainty (e.g., plume height, mass eruption rate and particle size distribution) are likely to dominate predictions of peak concentration and dosage. This suggests that, in the design of ensemble probabilistic forecasting methodologies, greater importance should be placed on quantifying eruption source uncertainty than structural uncertainty (provided suitable structural choices are made). When producing production guidance for quantitative forecasts for volcanic ash it would be advised that temporal and spatial averaging scales for the underlying dispersion simulations should also be specified.

This study uses meteorological data that is most suited to regional/intercontinental problems such as modelling the transport of radioactive isotopes following a nuclear accident and wheat rust spores. If higher resolution meteorological data was used then different structural choices maybe required to achieve the same accuracy in the dispersion forecasts. This maybe important for smaller scale phenomena such as airborne animal diseases, smoke from fires and chemical accidents. The results presented in this study are determined using a Lagrangian dispersion model which tracks particles to determine ash concentration. However, the results here relating to temporal and spatial resolution are applicable to Eulerian dispersion models, such as Ash3d (Schwaiger et al., 2012), for long-range applications.

This study could be expanded to consider a variety of different eruptions in different locations and to consider a range of flight routes. Additional work could also be performed to assess the relative importance of missing processes to the overall uncertainty in the ash forecasts. This work would hopefully be possible in the near future with the inclusion of new parameterization schemes for both aggregation and umbrella clouds in NAME (Beckett et al., 2022; Millward et al., 2023).

AUTHOR CONTRIBUTIONS

Lauren A. James: Methodology; software; validation; investigation; visualization; resources; writing – original draft; writing – review and editing. **Helen F. Dacre:** Conceptualization; methodology; writing – original draft; writing – review and editing; funding acquisition; supervision. **Natalie J. Harvey:** Conceptualization; methodology; software; resources; writing – original draft; writing – review and editing; supervision.

ACKNOWLEDGEMENTS

This work was funded by Lloyds Tercentenary Research Foundation.

CONFLICT OF INTEREST STATEMENT

The authors declare no conflict of interest. The funders had no role in the design of the study; in the collection, analyses or interpretation of data; in the writing of the manuscript, or in the decision to publish the results.

DATA AVAILABILITY STATEMENT

The data that support the findings of this study are openly available in University of Reading Research Data Archive at https://doi.org/10.17864/1947.000519.

ORCID

Lauren A. James https://orcid.org/0000-0002-7712-2837
Natalie J. Harvey https://orcid.org/0000-0003-0973-5794

REFERENCES

Beckett, F., Rossi, E., Devenish, B., Witham, C. & Bonadonna, C. (2022) Modelling the size distribution of aggregated volcanic ash and implications for operational atmospheric dispersion modelling. *Atmospheric Chemistry and Physics*, 22, 3409–3431.

Beckett, F.M., Witham, C.S., Leadbetter, S.J., Crocker, R., Webster, H.N., Hort, M.C. et al. (2020) Atmospheric dispersion modelling at the London VAAC: a review of developments since the 2010 Eyjafjallajökull volcano ash cloud. *Atmosphere*, 11, 352. Available from: https://www.mdpi.com/2073-4433/11/4/352

Bruckert, J., Hoshyaripour, G.A., Horváth, A., Muser, L., Prata, F.J., Hoose, C. et al. (2021) Online treatment of eruption dynamics improves the volcanic ash and so_2 dispersion forecast: case of the raikoke 2019 eruption. *Atmospheric Chemistry and Physics Discussions*, 2021, 1–23. Available from: https://acp.copernicus.org/preprints/acp-2021-459/

Capponi, A., Harvey, N.J., Dacre, H.F., Beven, K., Saint, C., Wells, C. et al. (2022) Refining an ensemble of volcanic ash forecasts using satellite retrievals: Raikoke 2019. *Atmospheric Chemistry and Physics*, 22, 6115–6134. Available from: https://acp.copernicus.org/articles/22/6115/2022/

Capponi, A., Harvey, N. J., Dacre, H. F., Beven, K., Saint, C., James, M. R., et al. (2022) *Ensembles of volcanic ash name simulations (01, 03, 08)*. Lancaster University. https://doi.org/10.17635/lancaster/researchdata/491

Clarkson, R. & Simpson, H. (2017) Maximising airspace use during volcanic eruptions: matching engine durability against ash cloud occurrence. In: *Proceedings of the NATO STO AVT-272 specialists meeting on: impact of volcanic ash clouds on military operations*. Vilnius, Lithuania: NATO STO AVT-272, pp. 15–17.

Clarkson, R.J., Majewicz, E.J. & Mack, P. (2016) A re-evaluation of the 2010 quantitative understanding of the effects volcanic ash has on gas turbine engines. *Proceedings of the Institution of Mechanical Engineers, Part G: Journal of Aerospace Engineering*, 230, 2274–2291. Available from: https://doi.org/10.1177/0954410015623372

Crawford, A. (2020) The use of gaussian mixture models with atmospheric lagrangian particle dispersion models for density estimation and feature identification. *Atmosphere*, 11. Available from: https://www.mdpi.com/2073-4433/11/12/1369

Crawford, A., Chai, T., Wang, B., Ring, A., Stunder, B., Loughner, C.P. et al. (2022) Evaluation and bias correction of probabilistic volcanic ash forecasts. *Atmospheric Chemistry and Physics*, 22, 13967–13996.

Dacre, H.F. & Harvey, N.J. (2018) Characterizing the atmospheric conditions leading to large error growth in volcanic ash cloud forecasts. *Journal of Applied Meteorology and Climatology*, 57, 1011–1019.

Dare, R.A., Smith, D.H. & Naughton, M.J. (2016) Ensemble prediction of the dispersion of volcanic ash from the 13 february 2014 eruption of kelut, Indonesia. *Journal of Applied Meteorology and Climatology*, 55, 61–78.

Denlinger, R.P., Pavolonis, M. & Sieglaff, J. (2012) A robust method to forecast volcanic ash clouds. *Journal of Geophysical Research-Atmospheres*, 117.

Folch, A. (2012) A review of tephra transport and dispersal models: evolution, current status, and future perspectives. *Journal of Volcanology and Geothermal Research*, 235-236, 96–115.

Folch, A., Costa, A. & Basart, S. (2012) Validation of the fall3d ash dispersion model using observations of the 2010 eyjafjallajökull volcanic ash clouds. *Atmospheric Environment*, 48, 165–183.

Global Volcanism Program. (2019a) Report on raikoke (Russia). In: crafford, A.E. & venzke, e. (Eds.) *Bulletin of the global volcanism network*, Vol. 44. Washington, DC: Smithsonian Institution, p. 8. Available from: https://doi.org/10.5479/si.GVP.BGVN201908-290250

Global Volcanism Program. (2019b) Report on raikoke (Russia). In: Sennert, S.K. (Ed.) *Weekly volcanic activity report, 19 June-25 June 2019*. Washington, DC: Smithsonian Institution and US Geological Survey.

Gouhier, M., Deslandes, M., Guéhenneux, Y., Hereil, P., Cacault, P. & Josse, B. (2020) Operational response to volcanic ash risks using hotvolc satellite-based system and mocage-accident model at the toulouse vaac. *Atmosphere*, 11, 864.

Harvey, N.J., Dacre, H.F., Saint, C., Prata, A.T., Webster, H.N. & Grainger, R.G. (2022) Quantifying the impact of meteorological uncertainty on emission estimates and the risk to aviation using source inversion for the Raikoke 2019 eruption. *Atmospheric Chemistry and Physics*, 22, 8529–8545. Available from: https://acp.copernicus.org/articles/22/8529/2022/

Harvey, N.J., Dacre, H.F., Webster, H.N., Taylor, I.A., Khanal, S., Grainger, R.G. et al. (2020) The impact of ensemble meteorology on inverse modeling estimates of volcano emissions and ash dispersion forecasts: Grímsvötn 2011. *Atmosphere*, 11, 1022. Available from: https://doi.org/10.3390/atmos11101022

Harvey, N.J., Huntley, N., Dacre, H.F., Goldstein, M., Thomson, D. & Webster, H. (2018) Multi-level emulation of a volcanic ash transport and dispersion model to quantify sensitivity to uncertain parameters. *Natural Hazards and Earth System Sciences*, 18, 41–63. Available from: https://nhess.copernicus.org/articles/18/41/2018/

Heard, I.P., Manning, A.J., Haywood, J.M., Witham, C., Redington, A., Jones, A. et al. (2012) A comparison of atmospheric dispersion model predictions with observations of SO_2 and sulphate aerosol from volcanic eruptions. *Journal of Geophysical Research-Atmospheres*, 117.

Hobbs, P.V., Radke, L.F., Lyons, J.H., Ferek, R.J., Coffman, D.J. & Casadevall, T.J. (1991) Airborne measurements of particle and gas emissions from the 1990 volcanic eruptions of mount redoubt. *Journal of Geophysical Research*, 96, 18735–18752.

International Civil Aviation Organization. (2022) Quantitative Volcanic Ash (QVA) Concentration Information. URL https://www.aviation.govt.nz/assets/licensing-and-certification/meteorology/QVA_information_flyer_vs_First-edition.pdf. First Edition

Jones, A., Thomson, D., Hort, M. & Devenish, B. (2007) The UK met office's next-generation atmospheric dispersion model, name iii. In: *Air pollution modeling and its application*, Vol. XVII. New York, NY: Springer, pp. 580–589.

Kristiansen, N., Stohl, A., Prata, A., Bukowiecki, N., Dacre, H., Eckhardt, S. et al. (2012) Performance assessment of a volcanic ash transport model mini-ensemble used for inverse modeling of the 2010 eyjafjallajökull eruption. *Journal of Geophysical Research-Atmospheres*, 117.

Lekki, J., Lyall, E., Guffanti, M., Fisher, J., Erlund, B., Clarkson, R. et al. (2013) Multi-partner experiment to test volcanic-ash ingestion by a jet engine. In: *6th international workshop on volcanic ash, no. GRC-E-DAA-TN8284*. Cleveland, OH: NASA, Glenn Research Center.

Mastin, L., Guffanti, M., Servranckx, R., Webley, P., Barsotti, S., Dean, K. et al. (2009) A multidisciplinary effort to assign realistic source parameters to models of volcanic ash-cloud transport and dispersion during eruptions. *Journal of Volcanology and Geothermal Research*, 186, 10–21. Available from: http://www.sciencedirect.com/science/article/pii/S0377027309000146

Mastin, L., Pavolonis, M., Engwell, S., Clarkson, R., Witham, C., Brock, G. et al. (2022) Progress in protecting air travel from volcanic ash clouds. *Bulletin of Volcanology*, 84, 9.

Millward, F.J., Webster, H.N. & Johnson, C.G. (2023) Modeling wind-blown umbrella clouds in lagrangian dispersion models. *Journal of Geophysical Research-Atmospheres*, 128, e2023JD039115. Available from: https://doi.org/10.1029/2023JD039115

Muser, L.O., Hoshyaripour, G.A., Bruckert, J., Horváth, A., Malinina, E., Wallis, S. et al. (2020) Particle aging and aerosol–radiation interaction affect volcanic plume dispersion: evidence from the raikoke 2019 eruption. *Atmospheric Chemistry and Physics*, 20, 15015–15036. Available from: https://acp.copernicus.org/articles/20/15015/2020/

Prata, A.T., Dacre, H.F., Irvine, E.A., Mathieu, E., Shine, K.P. & Clarkson, R.J. (2019) Calculating and communicating ensemble-based volcanic ash dosage and concentration risk for aviation. *Meteorological Applications*, 26, 253–266. Available from: https://doi.org/10.1002/met.1759

Prata, A.T., Grainger, R.G., Taylor, I.A., Povey, A.C., Proud, S.R. & Poulsen, C.A. (2022) Uncertainty-bounded estimates of ash cloud properties using the orac algorithm: application to the 2019 raikoke eruption. *Atmospheric Measurement Techniques*,

15, 5985–6010. Available from: https://amt.copernicus.org/articles/15/5985/2022/

Rougier, J. & Beven, K.J. (2013) Model and data limitations: the sources and implications of epistemic uncertainty. *Risk and Uncertainty Assessment for Natural Hazards*, 40, 40–63.

Schwaiger, H.F., Denlinger, R.P. & Mastin, L.G. (2012) Ash3d: a finite-volume, conservative numerical model for ash transport and tephra deposition. *Journal of Geophysical Research - Solid Earth*, 117. Available from: https://doi.org/10.1029/2011JB008968

Stefanescu, E., Patra, A., Bursik, M., Madankan, R., Pouget, S., Jones, M. et al. (2014) Temporal, probabilistic mapping of ash clouds using wind field stochastic variability and uncertain eruption source parameters: example of the 14 a pril 2010 E yjafjallajökull eruption. *Journal of Advances in Modeling Earth Systems*, 6, 1173–1184.

Walters, D., Baran, A.J., Boutle, I., Brooks, M., Earnshaw, P., Edwards, J. et al. (2019) The met office unified model global atmosphere 7.0/7.1 and jules global land 7.0 configurations. *Geoscientific Model Development*, 12, 1909–1963.

Webster, H.N. & Thomson, D.J. (2022) Using ensemble meteorological data sets to treat meteorological uncertainties in a bayesian volcanic ash inverse modeling system: a case study, grímsvötn 2011. *Journal of Geophysical Research-Atmospheres*, 127, e2022JD036469. Available from: https://doi.org/10.1029/2022JD036469

Webster, H.N., Thomson, D.J., Johnson, B.T., Heard, I.P.C., Turnbull, K., Marenco, F. et al. (2012) Operational prediction of ASH concentrations in the distal volcanic cloud from the 2010 Eyjafjallajökull eruption: PREDICTING EYJAFJALLAJÖKULL ASH LEVELS. *Journal of Geophysical Research*, 117. Available from: https://doi.org/10.1029/2011JD016790

Witham, C., Hort, M., Potts, R., Servranckx, R., Husson, P. & Bonnardot, F. (2007) Comparison of vaac atmospheric dispersion models using the 1 november 2004 grimsvötn eruption. *Meteorological Applications: A Journal of Forecasting, Practical Applications, Training Techniques and Modelling*, 14, 27–38.

Witham, C., Hort, M., Thomson, D., Devenish, B., Webster, H. & Beckett, F. (2019) The current volcanic ash modelling set-up at the London VAAC.

Zidikheri, M.J. & Lucas, C. (2021) A computationally efficient ensemble filtering scheme for quantitative volcanic ash forecasts. *Journal of Geophysical Research-Atmospheres*, 126, e2020JD033094.

How to cite this article: James, L. A., Dacre, H. F., & Harvey, N. J. (2024). How dependent are quantitative volcanic ash concentration and along-flight dosage forecasts to model structural choices? *Meteorological Applications*, *31*(5), e70003. https://doi.org/10.1002/met.70003